Chemistry–A European Journal
Research Article
doi.org/10.1002/chem.202301036
Chemistry Europe
European Chemical Societies Publishing
www.chemeurj.org

Special Collection

Metal-Free Electrocatalysts for the Selective 2e⁻ Oxygen Reduction Reaction: A Never-Ending Story?

Giulia Tuci,*[a] Andrea Rossin,[a] Xiong Zhang,[b, c] Lai Truong-Phuoc,[b] Enrico Berretti,[a] Yuefeng Liu,[d] Cuong Pham-Huu,[b] Sajjad Ali,[e] Faheem Jan,[f] Lorenzo Poggini,[a] and Giuliano Giambastiani*[a]

Dedicated to Prof. Maurizio Prato on the occasion of his 70th birthday

Abstract: Hydrogen peroxide (H_2O_2) electrosynthesis via the 2e⁻ Oxygen Reduction Reaction (ORR) represents a highly challenging, environmentally friendly and cost-effective alternative to the current anthraquinone-based technology. Various lightweight element hetero-doped carbon nanostructures are promising and cheap metal-free electrocatalysts for H_2O_2 synthesis, particularly those containing O-functionalities. The exact role of O-containing functional groups as electroactive sites for the process remains debated if not highly controversial. Herein, we have reported on the covalent exohedral functionalization of the outer surface of extra-pure multi-walled carbon nanotubes (MWCNTs) with discrete O-functional groups as a unique approach to prepare selective electrocatalysts for the process. This kind of decoration has added fundamental tiles to the puzzling structure/reactivity relationship of O-containing carbon-based catalysts for ORR, clearing doubts on the controversial role of hydroxyl/phenol groups as key functionalities for the design of more performing 2e⁻ ORR electrocatalysts.

Introduction

Hydrogen peroxide (H_2O_2) is among the 100 most important chemicals in the world,[1] with a global market close to 1.7 billion USD in 2021 and a forecasted growth up to 2.2 billion USD by 2028. It is a green oxidant and a bleaching agent classically used in the modern chemical, textile, sanitary and cosmetic industry as well as a chemical agent for addressing environmental and sanitary challenges.[2–3] COVID-19 pandemic has certainly boosted H_2O_2 production as antiseptic. At the same time, the search for sustainable energy production methods based on the conversion of chemical energy into electrical energy has drawn the attention on the practical use of hydrogen peroxide as a solar fuel within simplified fuel cell devices.[4]

Current H_2O_2 large-scale production methods are based on the multi-step and energy-intensive anthraquinone process. Centralized plants have been developed where highly expensive palladium-based catalysts are employed and large quantities of by-products are generated.[5] The missing of simplified and cheaper hydrogen peroxide "on-site production technologies" together with its hazardous nature and related handling, transportation and storage concerns have increased H_2O_2 production costs.[6] In recent years, the selective electrocatalytic oxygen reduction reaction (ORR) has powerfully emerged as an on-site, cost-saving and greener (without organic wastes) technology to replace the anthraquinone process in H_2O_2 production.[2,7–10] Moreover, the combination of the electrochemical technology with renewable electricity sources (*i.e.*, solar, wind) makes the approach even more sustainable with respect to the current production methods based on the use of

[a] Dr. G. Tuci, Dr. A. Rossin, Dr. E. Berretti, Dr. L. Poggini, Dr. G. Giambastiani
Institute of Chemistry of OrganoMetallic Compounds
ICCOM-CNR and Consorzio INSTM
Via Madonna del Piano, 10 – 50019, Sesto F.no, Florence (Italy)
E-mail: giulia.tuci@iccom.cnr.it
giuliano.giambastiani@iccom.cnr.it

[b] Dr. X. Zhang, Dr. L. Truong-Phuoc, Dr. C. Pham-Huu
Institute of Chemistry and Processes for Energy
Environment and Health (ICPEES), ECPM, UMR 7515
CNRS-University of Strasbourg
25 rue Becquerel, 67087 Strasbourg Cedex 02 (France)

[c] Dr. X. Zhang
CAS Key Laboratory of Science and Technology on Applied Catalysis
Dalian Institute of Chemical Physics, Chinese Academy of Sciences
116023 Dalian (China)

[d] Prof. Y. Liu
Dalian National Laboratory for Clean Energy (DNL)
Dalian Institute of Chemical Physics
Chinese Academy of Science
457 Zhongshan Road, 116023 Dalian (China)

[e] Dr. S. Ali
Yangtze Delta Region Institute (Huzhou)
University of Electronic Science and Technology of China
Huzhou 313001 (China)

[f] F. Jan
Institute of Metal Research, Chinese Academy of Sciences
Shenyang 110016 (China)

Supporting information for this article is available on the WWW under https://doi.org/10.1002/chem.202301036

This article is part of a joint Special Collection in honor of Maurizio Prato.

fossil fuels.[11] This approach to H_2O_2 production perfectly matches with the *e*-catalysis concept linked to one priority transition of modern chemical industry towards fossil fuels-free technologies.[12] To date, the biggest research efforts driven by the market of metal-air batteries and fuel cell devices have pointed to the design and synthesis of efficient and durable noble-metal based electrocatalysts (e.g., Pt, Pd, Au and their alloys) for O_2 conversion to H_2O or hydroxide ions (OH^-) through a complete $4e^-$ reduction path.[13–14] Selected electrocatalysts from this series are highly performing for the $2e^-$ reduction path as well, to give H_2O_2 or HOO^- ions selectively. Anyhow, their high costs and scarce availability on the global market primarily hamper any practical and large-scale exploitation.[15–18] Metal-free carbon-based porous architectures in the form of lightweight element hetero-doped networks (mainly containing N, O and S) have gained the attention of the catalysis community as effective (electro)catalysts for a number of key industrial transformations.[19–20] Seminal studies on this field have unveiled the existence of an efficient, selective, cheap and abundant alternative to the use of noble metal-based catalysts for the $4e^-$[21–23] and $2e^-$ ORR.[24–30] As far as the latter is concerned, O-containing groups as surface dopants of various carbon allotropes have unveiled their superior aptitude to drive ORR towards a preferential $2e^-$ reduction process.[7,31–40] In spite of promising catalytic outcomes, many efforts are still necessary to better control the process selectivity and to establish a clear-cut structure/reactivity relationship for this class of metal-free systems.

"Bottom-up" synthetic strategies applied to the production of O-enriched C-nanomaterials typically result in complex systems containing multiple O-functionalities (ketones, ethers, carboxylic acids) together in the same material. As a result, any attempt to speculate on their different role on the ORR selectivity ($4e^-$ vs. $2e^-$ reduction process) remains highly speculative. Tailored synthetic strategies[34,39] often corroborated by DFT predictions[31,36] and eventually combined with titration post-synthetic procedures for the targeted quenching of selected functionalities (i.e., C=O, C–OH or COOH)[35] have been exploited for a rational tuning of the nature/composition of O-dopants at the C-nanomaterials surface.[32] These approaches have shed light on a highly controversial issue, although the ultimate role of each O-containing group on the selective $2e^-$ ORR path remains a matter of debate for the scientific community, being a never-ending source of conflicting literature outcomes. In particular, carboxyl (–COOH),[31,36,41] ether (C–O–C)[34,38] or carbonyl/quinone (C=O)[32,35,37,41] groups have been claimed - time to time - as the most active O-functionalities for the selective $2e^-$ ORR.

The exohedral decoration of carbon nanomaterials with selected functional groups is a powerful "top-down" approach for the control of the chemical and electronic nature of surface dopants. It has certainly contributed to unveil the role of well-defined heteroatom-containing functional groups engaged in selected (electro)catalytic processes.[42–43] Such an approach has already been successfully exploited by some of us for the comprehension of the reaction mechanisms promoted by these metal-free systems in the activation and conversion of challenging small molecules.[44–49]

Herein, we have conveniently extended our exohedral functionalization protocol to the synthesis of a series of multi-walled carbon nanotubes (MWCNTs) decorated with well-defined O-containing dangling arms (i.e., carboxyl, carbonyl, ether and phenol/hydroxyl groups). Accordingly, oxygenated organic fragments with different chemico-physical properties (i.e., polarity, acidity) and affinity for the reaction medium have been grafted to the MWCNTs surface (Scheme 1); the resulting derivatives have been exploited as metal-free electrocatalysts in the $2e^-$ ORR under alkaline environment. In contrast with a very recent report dealing with the electrocatalytic performance of tightly related functional materials,[40] our findings have unambiguously demonstrated the superior performance (onset potential and H_2O_2 selectivity) of metal-free systems containing dangling phenol groups (–C_6H_4–OH; **5**). Finally, a comparative analysis with other O-functionalized samples (–C_6H_4–CO–Ph, **6**; –C_6H_4–O–Ph, **7**; –C_6H_4–COOH, **8**) has served to narrow the field down to the most active groups engaged in the selective$2e^-$ ORR.

Results and Discussion

Synthesis and characterization of MW/$C_6H_4R_{1-4}$ samples (5–8)

Four novel functionalized MWCNT samples have been prepared under mild experimental conditions starting from ultra-pure MWCNT samples (>98% C) and the aniline derivatives (**1**–**4**) under the classical aryl-diazonium salt conditions (Tour-protocol, Scheme 1).[50–51] Samples containing various O-functionalities (*i.e.*, alcohols, carbonyls, ethers and carboxylic acids) have been isolated in the form of phenol (MW/C_6H_4OH, **5**), benzophenone (MW/C_6H_4COPh, **6**), diphenyl-ether (MW/C_6H_4OPh, **7**) and benzoic acid (MW@C_6H_4COOH, **8**) dangling moieties, respectively.

Each sample underwent a careful workup procedure through successive sonication/centrifugation and filtration treatments to remove all traces of unreacted reagents (see Experimental Section for details). In addition, a *blank* reaction

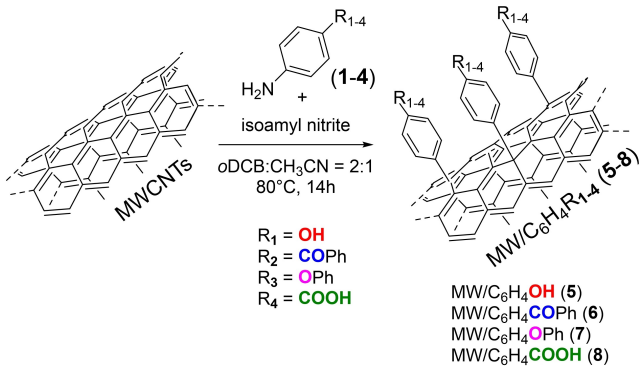

Scheme 1. Exohedral functionalization of MWCNTs with variably O-containing aniline derivatives (**1**–**4**).

test was carried out with each aniline sample (**1**–**4**) but in the absence of the isoamyl nitrite as activator. These *blank* samples were regularly worked-up and employed in turn for quantifying the physisorbed N-containing residues, hence ruling out any potential electrochemical contribution from these contaminants. The quantitative assessment of the functionalization degree for purely C- and O-containing fragments at the surface of macromolecular C-derivatives (**5**–**8**) is other than obvious. This is due to the moderate accuracy offered by the analytical tools for measuring the loading of light hetero-elements (e.g., O), what's more in low-charged samples. A semiquantitative estimation was preliminarily assessed from the thermogravimetric analysis of **5**–**8** and pristine MWCNTs under N_2 atmosphere. As Figure 1 shows, all thermograms showed from moderately to appreciably high weight losses with respect to pristine MWCNTs in the 40–550 °C temperature range. At higher temperature values, thermograms show largely superimposable decomposition trends. To roughly estimate the loading of each grafted aryl group, the weight loss measured for MWCNTs between 40 and 550 °C was subtracted by that of each functionalized sample in the same range of temperatures.

Expectedly, the higher the stability of the reactive aryl radical intermediate formed by the anilines activation,[50–51] the lowest its reactivity and the functionalization degree in the final product. Accordingly, the activation of **2** by the isoamyl-nitrite gives rise to a highly conjugated and stable aryl radical that translates into an only moderate functionalization degree (sample **6**).

Elemental analysis (EA) of **5**–**8** and their *blank* counterparts excluded the presence of unreacted reagents (aniline, isopentyl-nitrite) and solvents (CH_3CN) as contaminants (Table 1). In particular, the missing of N-containing species excludes aniline residues simply adsorbed on the *blank* and functionalized materials. The decrease of carbon content measured in **5**–**8** is an indirect proof of surface grafting by O-containing moieties; the higher the O/C ratio of grafted fragments and their supposed functionalization degree (Table 1), the lowest the absolute C/C ratio between samples **5**–**8** and their *blank* counterparts.

XPS data of pristine and functionalized MWCNTs have provided additional details on the samples chemical composition. Survey spectra were consistent with the expected elemental composition (C and O only) of each functionalized material while confirming the absence of N- or halo-containing contaminants (*i.e.*, oDCB). Distinctive components in the peak-fitting of the high-resolution O1s core regions have qualitatively

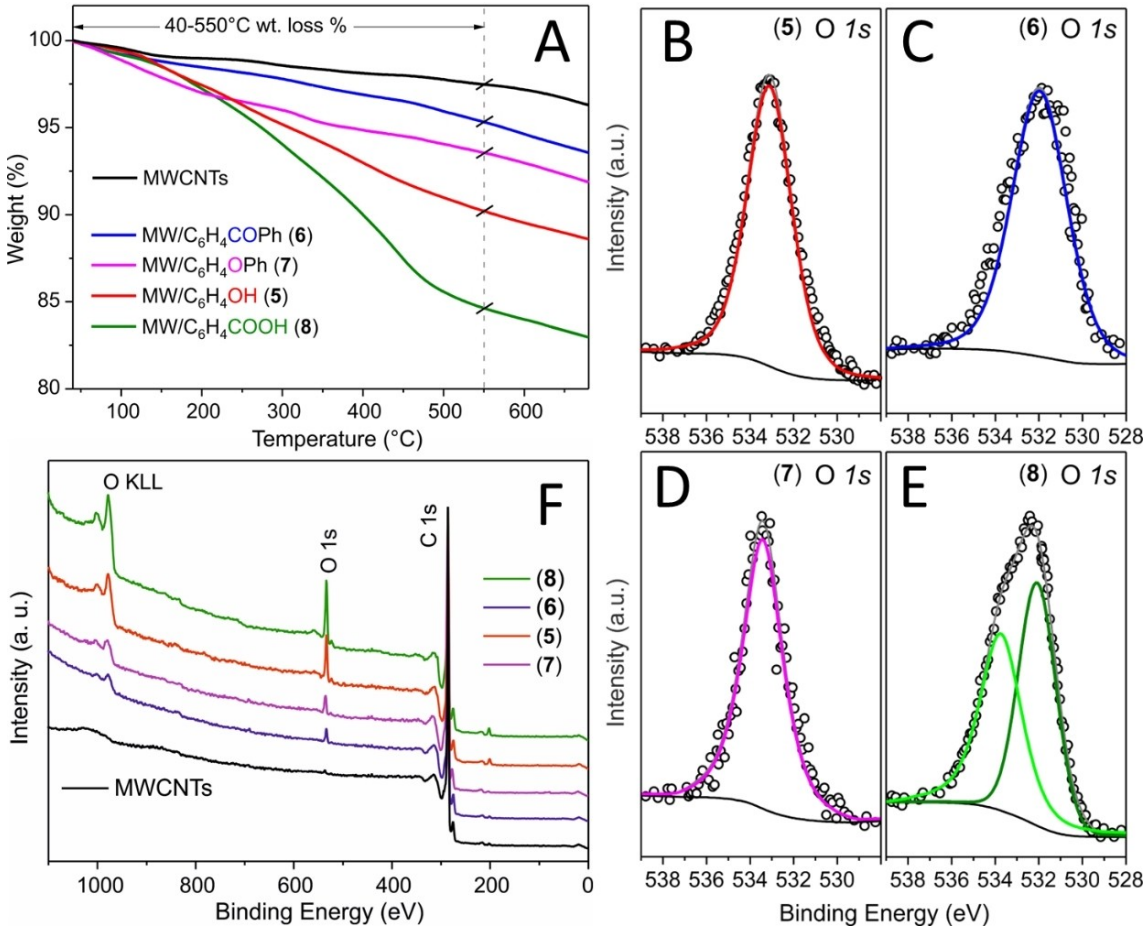

Figure 1. A) Thermogravimetric profiles of samples **5**–**8** and pristine MWCNTs; analysis conditions: 40–700 °C, 5 °C/min, N_2 atm., 100 mL min^{-1}. B–E) XPS high resolution O1s core regions of samples **5**–**8**. F) XPS survey spectra of samples **5**–**8** and pristine MWCNTs. All survey spectra are normalized to the C1s peak.

Table 1. TGA, EA, acid-base titration and EDX data of samples **5**–**8** at comparison with pristine MWCNTs.

Sample	TGA		EA[c]			Titration		EDX	
	wt. loss [%][a]	[mmol g^{-1}][b]	C [%]	H [%]	N [%]	O [wt.%]	[mmol g^{-1}][d]	O [wt.%][e]	[mmol g^{-1}]
MWCNTs	2.52	–	98.55	0.03	–	–	–	0.08	0.05
(**5**)	9.66	0.76	86.78	0.92	–	1.09	0.68	0.82	0.46[g]
blank test[f]	n.d.	n.d.	94.55	0.32	–	–	–		–
(**6**)	4.69	0.12	92.67	0.49	–	–	–		–
blank test[f]	n.d.	n.d.	95.54	0.26	–	–	–		–
(**7**)	6.45	0.23	90.88	0.62	–	–	–		–
blank test[f]	n.d.	n.d.	94.96	0.22	–	–	–		–
(**8**)	15.37	1.05	84.58	0.88	–	3.81	1.19	4.62	1.42[g]
blank test[f]	n.d.	n.d.	94.53	0.26	–	–	–		–

[a] wt.% loss measured in the 40–550 °C temperature range; measures were run under a constant N_2 stream (100 mL min^{-1}). [b] Functional group loading estimated assuming a sample weight loss given by the difference between the functionalized material and MWCNTs in the 40–550 °C temperature range. [c] C, H and N % calculated as average values over three independent runs. [d] Acid sites loading estimated over three independent measurements. [e] Average value from three independent spots. [f] Sample obtained using identical reaction conditions, reagents and work-up procedure applied to samples **5**–**8**, except for the use of the isoamyl nitrite as reagent. [g] Functional group loading calculated subtracting the O-contribution from pristine MWCNTs.

confirmed the nature of the O-containing grafted groups at the CNT surface. Accordingly, the O1s curve fitting has unveiled the presence of hydroxyl (–OH, BE = 533.3 ± 0.2 eV),[52–54] carbonyl (C=O, BE = 531.9 ± 0.2 eV),[31,52,54–55] ether (C–O–C, BE = 533.4 ± 0.2 eV)[31,54] and carboxyl (–COOH, $BE^{C=O}$ = 532.1 ± 0.2 eV and BE^{C-OH} = 533.7 ± 0.2 eV)[56] functionalities in **5**, **6**, **7** and **8**, respectively. No quantitative information on the samples functionalization degree has been gained from XPS data, except for an O-content trend in **5**–**8** coherent with the semiquantitative functionalization data obtained from TGA. Figure 1F illustrates this O-trend for C-normalized survey spectra, magnified along the Y axis.

For **5** and **8**, the presence of proton-labile groups (–OH and –COOH) has been exploited for quantitative purposes. Therefore, an acid-base titration (see Experimental Section for details) has been carried out and a new functionalization loading has been fixed for these two samples at least.

Loading values measured on both functionalized materials varied moderately (ca. ±10%) with respect to those derived from thermogravimetric outcomes. As an additional trial, EDX analysis on the same samples has unveiled similar but more pronounced discrepancies in O-contents (Table 1).

Although any clear-cut quantitative conclusion on the functional group loading of samples **5**–**8** remains hard to be drawn, all data taken together appear coherent and confirm the existence of a functionalization trend. **8** is the most functionalized (benzoic acid) material, followed by **5** with an intermediate loading of phenolic pendant arms and by **6**–**7** (ketones and ethers) with the lowest functionalization degree.

Two representative samples from this series (*i.e.*, pristine MWCNTs and **8** with the higher surface functionalization degree) were analyzed through high-resolution transmission electron microscopy (TEM) to confirm the non-invasive character of the functionalization path. Except for a superior CNTs bundle disaggregation in the functionalized sample **8**, both materials showed virtually unchanged morphological properties (length and diameter) (Figure S1 vs. S2). Previous studies based on Raman spectroscopy of related functionalized CNTs have shown only negligible alterations of the Raman D and G modes caused by the covalent surface grafting.[44–45] Therefore, the highly defective surface (and bulk) site density of pristine MWCNTs makes any Raman characterization meaningless.

Specific surface area (SSA), total pore volume and pore-size distribution have been measured through N_2 physisorption analysis at the liquid N_2 temperature (−196 °C) on all functionalized samples and their blank counterparts (Table S1). This analysis has assessed the role of surface functionalization on the ultimate CNT morphology and it has unveiled the existence of preferred CNT portions where the exohedral functionalization occurs. Figure S3 outlines the Type II isothermal profiles typical of mesoporous networks featured by complex pore structures of ill-defined shape of the most catalytically representative sample **5** (see below) and its *blank* counterpart.[57] Notably, smaller mesopores are completely suppressed in **5** and its SSA is roughly reduced by 20% (from 187 of *blank* sample to 149 m^{2}g^{-1}). Accordingly, functionalization is likely to take place preferentially on the smaller mesopores where highly defective, bent and reactive C–C structures are present.

All electrochemical ORR tests carried out on **5**–**8** (including pristine MWCNTs) were accomplished using a constant sample weight (see Experimental Section) to fabricate Nafion-based inks and the related electroactive thin films.

Electrochemical tests on 5–8 as ORR catalysts for a prevalent 2 e$^-$ reduction path

Electrocatalysts **5**–**8** and pristine MWCNTs have been scrutinized as potentially selective systems for the challenging 2e$^-$ Oxygen Reduction Reaction (ORR) to hydrogen peroxide (H_2O_2). To this aim, a Nafion®-based ink was prepared with each sample and dropcasted on the glassy carbon disk of a rotating ring-disk electrode (RRDE). Each deposit of the electroactive phase was realized using a constant material concentration (5 mg of CNT-derivative in 1.05 mL of solution) to get thin and homogeneous film deposits after solvent evaporation (Working Electrode - WE, see Experimental Section for details). Each WE was employed in a three electrodes cell equipped with an Ag/AgCl/$KCl_{sat.}$ and a

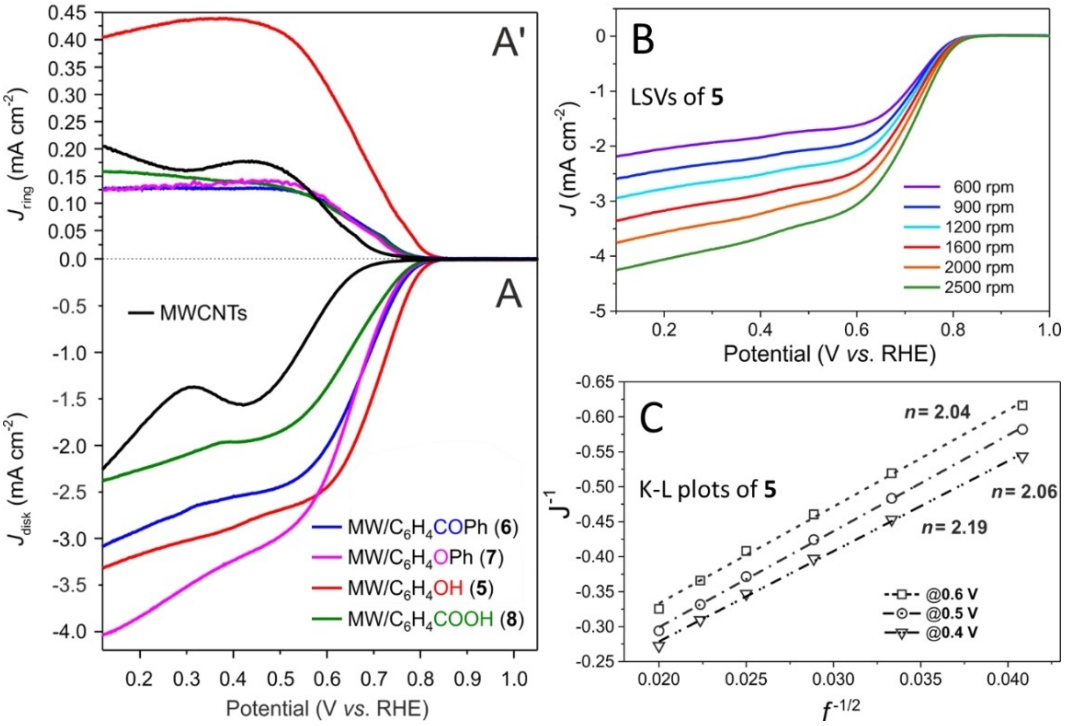

Figure 2. A) Disk and A') Pt-ring RRDE Linear Sweep Voltammograms (LSVs) of samples **5**–**8** and MWCNTs registered in an O_2-saturated 0.1 M KOH aqueous solution at an electrode spin rate of 1600 rpm. B) LSVs of **5** at variable electrode rotation speed (600–2500 rpm) and C) related K-L plots measured at three different potential values (0.4–0.6 V).

graphite rod as the reference and counter electrode, respectively. RRDE voltammograms of all decorated materials (**5**–**8**) and pristine MWCNTs were recorded under an O_2-saturated 0.1 M KOH electrolyte solution (alkaline environment). Linear Sweep Voltammograms (LSVs) were recorded at 1600 rpm while sweeping the applied potential values linearly from 0.1 to 1.1 V vs. RHE. Background currents were then measured under saturated N_2 conditions and subtracted from the respective curves to eliminate all capacitive contributions. **5**–**8** presented distinctive profiles with a markedly positive shift of the disk onset potential (E_{on} - Disk) with respect to that of pristine MWCNTs (Figure 2A and Table 2). Notably, **5** displayed a shift of about + 150 mV (0.82 V vs. RHE) with respect to plain MWCNTs and up to + 20–30 mV with respect to all other exohedrally functionalized materials from this series (**6**–**8**; Table 2). The E_{on} gap among the functionalized samples was even higher for the current density profiles measured at the Pt ring of the RRDE electrode and directly associated to the production of hydrogen peroxide (Figure 2A'). The onset potential (E_{on} - Ring) of **5** (0.82 V vs. RHE) was up to 40–60 mV higher than that recorded on **6**–**8** (Table 2).

Table 2. Disk and Pt-ring onset potential values (E_{on}), H_2O_2 (%) produced and number of electrons exchanged (n) *per* O_2 molecule for samples **5**–**8** along with plain MWCNTs.

Sample	E_{on} [V]$_{disk}$[a]	E_{on} [V]$_{ring}$[b]	H_2O_2 [%][c]	n[c]
MWCNTs	0.67	0.64	66	2.67
5	0.82	0.82	79	2.41
6	0.80	0.78	31	3.38
7	0.80	0.76	29	3.42
8	0.79	0.77	41	3.19

[a] Potential at $J_{disk} = -0.05$ mA/cm^2. [b] Potential at $J_{ring} = 0.015$ mA/cm^2. [c] Estimated from ring/disk current values at 0.5 V vs. RHE.

Noteworthy, **5** shows markedly higher current density values measured at the Pt-ring of the RRDE, consistent with a net and superior hydrogen peroxide production within the whole range of scanned potential values. J_{ring} values of **5** at selected potentials are more than doubled if compared with those of the other functionalized samples from this series (**6**–**8**, Figure 2A'). Accordingly, hydrogen peroxide selectivity calculated for **5** [H_2O_2 (%) - Table 2 and Figure S4] is close to 80%, hence unveiling a prevalent 2e$^-$ reduction process at work. In contrast, functionalized samples **6**–**8** that produce H_2O_2 to a lower extent (Table 2) favor a prevalent 4e$^-$ reduction pathway towards hydroxide ions (OH^-). A careful analysis of the voltametric profiles for each electrocatalyst has pointed out the superior performance of **5** towards a 2e$^-$ ORR to H_2O_2. At odds with plain MWCNTs and samples **6**–**8**, H_2O_2 production on **5** starts simultaneously ($E = 0.82$ V vs. RHE) with the reduction process. Indeed, E_{on} values measured for this electrocatalyst at the disk and Pt-ring are identical. On the other hand, a + 20–40 mV E_{on} overpotential at the Pt-ring with respect to the E_{on} disk-value is recorded for all the other functionalized samples **6**–**8**.

The superior performance of **5** in promoting O_2 reduction to hydrogen peroxide mainly (2e$^-$ ORR) has also been confirmed

by the calculation of the number of transferred electrons per O_2 molecule (*n*) through the Koutecky-Levich model. K-L plots obtained from LSVs recorded on **5** at variable electrode spin rates (Figure 2B) account for an average value of 2.1e$^-$ transferred *per* O_2 molecule in the 0.4–0.6 V potential range vs. RHE (Figure 2C). This value corresponds to an electrode ORR selectivity towards hydrogen peroxide of *ca.* 90%. In spite of the known intrinsic limits of the used analytical methods (J_{ring} in RRDE vs. K-L model) responsible for not-negligible differences in the estimated H_2O_2 selectivity,[58] the K-L model further confirms the superior ability of **5** to promote ORR via a prevalent (selective) 2e$^-$ reduction path. For the sake of completeness, LSVs for all other electrocatalysts and the relative K-L model with the average number of electrons (*n*) exchanged per O_2 molecule are outlined in Figure S5.

All these data taken together suggest that surface functionalization with tailored O-containing functionalities can be hardly claimed as a prerequisite to impart a higher electrochemical activity to MWCNT-derivatives towards a selective 2e$^-$ ORR. A different functional group loading [MW/C_6H_4COOH (**8**) $\gg$ MW/C_6H_4COPh (**6**)] or the superior affinity of surface hydrophilic groups towards the reaction medium (and the subsequent superior nanomaterial dispersibility) [MW/C_6H_4COOH (**8**) > MW/C_6H_4COPh (**6**) = MW/C_6H_4OPh (**7**)] do not seem to impact on the electrochemical performance appreciably. In addition, an only moderate alteration of pore size distribution and SSA of functionalized materials vs. plain ones seems to exclude an active role of these morphological properties on the catalysts ultimate electrochemical performance. Lastly, any contamination of the electroactive materials by adventitious metals or metal-residues (from the catalytic CNT production) suitable to impart the observed electrochemical outcomes can be ruled out. Indeed, the proposed top-down functionalization approaches occur through mild and metal-free protocols and allow for a direct electrochemical comparison of the surface functionalized C-networks with their unfunctionalized counterparts. The analysis of the latter excludes any electrochemical activity ascribable to metal-catalyst residues rising from the MWCNTs synthesis.

Overall, the grafting of MWCNTs with phenol dangling moieties (**5**) boosted appreciably the process selectivity towards the production of hydrogen peroxide (2e$^-$ ORR) (Figure 2A, A′ and Table 2). This functionalized material has unveiled comparable[32,35–36,38–39] or even superior[31,34,37,40] performance (E_{on} - disk and E_{on} - ring) with respect to those from the literature dealing with O-doped carbon nanomaterials as metal-free systems operating under comparable experimental conditions. For the sake of completeness, we have finally performed a stability test on **5** as the most representative electrocatalyst from this series. To this end, **5** was cycled under oxygen saturated atmosphere for about 1000 electrochemical runs in the 0.1 ÷ 0.9 V range vs. RHE (see Figure S6 and experimental section for details). Figure S6 shows the current density stabilization (J_{disk}) on the metal-free catalyst that rapidly and almost asymptotically lies around $-2.76\ mA\,cm^{-1}$ already after 300 cycles, with an estimated J_{disk} decrease (measured at 0.4 V vs. RHE) of less than 5% on the whole test duration. This experiment confirms the excellent catalyst stability and durability under the operative experimental conditions.

Evidences based on the tailored functionalization of MWCNTs with discrete and surface exposed O-containing functional groups allow to better speculate on the effective nature of the active sites engaged in the process. At the same time, they contribute to clarify the controversial role of various O-containing groups (i.e., –COOH, –OH, ethers and ketones) often invoked as key systems for a 2e$^-$ ORR under alkaline environment. In contrast to recent reports on related O-doped carbon nanomaterials[31,59] as selective electrocatalysts for the 2e$^-$ ORR, activity and selectivity in the process do not linearly correlate with the materials O-content but rather with the chemical nature and specific electronic properties of the active sites. This evidence shines through the comparative electrochemical performance of the two model samples (**5** and **8**) from our series. In spite of a comparable dispersibility of **5** and **8** in alkaline media, their virtually comparable morphological properties and the superior functionalization loading (and O-content) of **8** (1.05 mmol/g, TGA from Table 1) vs. **5** (0.76 mmol/g, TGA from Table 1), the latter outperforms **8** and all the other functionalized materials from the series in the 2e$^-$ ORR.

It can be inferred that the superior performance of **5** is linked to the electronic properties of the surface exposed phenol groups and their inherent aptitude to stabilize a first proton-coupled electron transfer in the form of the key intermediate HOO* [Eqs. (1) and (2)]. A second electron acceptance completes the reduction process and releases hydrogen peroxide [Eq. (3), right-hand side]. The 4e$^-$ reduction path occurs through the competitive O–O dissociation of the activated HOO* species into OH^- and O* [Eq. (3), left-hand side]. This second electron transfer thus depends on the favored reaction path to which HOO* undergoes and thus on the stabilization effect played by the different electronic microenvironment originated at the various O-containing groups available on the nanomaterial surface.

$$O_2(g) + {}^* \rightarrow O_2^* \tag{1}$$

$$O_2^* + H_2O(l) + e^- \rightarrow HOO^* + OH^- \tag{2}$$

$$OH^- + O^* \leftarrow [HOO^* + e^-] \rightarrow HOO^- + {}^* \quad (2e^-\ path) \tag{3}$$

$$O^* + H_2O(l) + 2e^- \rightarrow 2OH^- + {}^* \quad (4e^-\ path) \tag{4}$$

Therefore, a selective electrocatalyst for H_2O_2 production will disfavor the O–O bond cleavage, i.e., it will adsorb O_2 strongly enough to promote the first reduction to HOO* while binding the latter weakly enough to allow the hydrogen peroxide ion desorption before O–O dissociation takes place.[24,32,35]

C-atoms neighboring electron-rich hetero-dopants (i.e., C_α in O- and N-containing functional groups mainly) are classically invoked as the active sites suitable to reversibly bind/activate dioxygen or its reduced intermediates with variable strength at

the origin of the observed process selectivity.[31–32] As for samples featured by proton-labile groups and closest dispersibility/wettability towards the alkaline aqueous environment (e.g., **5** and **8**), the selectivity is likely controlled by the different electron density at the C_α to oxygen(s) atom(s). Evidences lead to conclude that C_α to hydroxyl groups of phenols (**5**) ensures a most favorable interaction with dioxygen than C_α of carboxylic acids (**8**). Indeed, the former boosts the first electron transfer already at low overpotential values (0.82 V vs. RHE, E_{on} - disk, Table 2) and binds the key intermediate HOO* with the "appropriate" strength for the second electron transfer that occurs at the same potential (0.82 V vs. RHE, E_{on} - ring, Table 2). Finally, C_α in **5** quickly releases HOO^- ions [$2e^-$ path; Eq. (3)], hence limiting the occurrence of the O–O bond breaking side-process [$4e^-$ path; Eq. (4)].

Some of us have already discussed similar C_α-electronic effects in terms of relative electron density distribution (calculated through the Bader charge analysis) in N-containing organic groups grafted at the surface of MWCNTs and engaged as metal-free electroactive sites for the $4e^-$ ORR.[44–45] The Bader charge analysis applied to the simplified model systems **5'**-**8'** after a preliminary structure optimization (Figure S7 and Experimental section) proves the floating electronic density at the O-neighboring C-atoms likely engaged in the process and casts light on their role in the $2e^-$ ORR. A direct relationship between the C_α charges and the catalytic activity is found, in line with the experimental data. The best performing sample **5** is featured by the combination of an intermediate positive charge on its C_α atom ($qC_\alpha = +0.52$) and a good wettability in aqueous environment that together boost the $2e^-$ ORR. Samples **6** and **7** featured by a higher ($qC_\alpha = +0.99$) and lower (mean $qC_\alpha = +0.39$) Bader C_α charge and reduced water affinity are less efficient and selective $2e^-$ ORR catalysts. Despite the excellent water affinity of the more copious carboxylic acid groups in **8**, the higher Bader C_α charge ($qC_\alpha = +1.51$) is thought to hamper the release of the reaction intermediate HO_2^-, too tightly bound to the dangling O-bearing group. Consequently, its ORR performance is lower than that of **5**.

Conclusions

New insights to the hitherto not fully clarified nature of O-containing functional groups as surface active-sites in metal-free electrocatalysts for the selective $2e^-$ ORR have been provided. Exohedrally functionalized multi-walled carbon nanotubes with tailored and surface exposed O-containing functionalities (phenol, benzophenone, diphenyl-ether or benzoic acid groups) have been conveniently synthesized by the aryl-diazonium salt protocol. Individual hydroxyl-, carbonyl-, ether- and carboxyl-groups as surface dangling arms of complex carbon nanostructures have then been scrutinized as electroactive sites for a prevalent O_2 reduction path to HO_2^- ions under alkaline environment. The "top-down" functionalization approach to electrocatalysts synthesis allows for an exclusive control of the chemical and electronic properties of surface-grafted groups. At odds with the general perception of nanocarbons syntheses as highly batch-dependent materials, this protocol guarantees high synthetic reproducibility and allows to exclude any electro-catalytically active contribution other than that of plain O-containing functionalities. It allows for a better speculation on the chemical and electronic properties of unique and surface exposed groups engaged in the reduction process. Accordingly, phenols have shown superior performance in the dioxygen activation for their selective $2e^-$ reduction to hydrogen peroxide. In contrast with all other surface O-functionalities in the study (**6**-**8**), phenols (**5**) realize an ideal chemical and electronic microenvironment suitable for the first electron transfer process to take place. Phenol binds the ORR intermediate HOO* with the "appropriate" strength to facilitate a second electron transfer and concomitant HO_2^- release ($2e^-$ path). At the same time, the O–O dissociation path ($4e^-$ reduction) is strongly limited.

If tailored metal-free electrocatalysts from this series and their electrochemical outcomes serve to better elucidate the role of O-containing functionalities in the challenging O_2-to-H_2O_2 reduction process, they also spot-light on the delicate electronic balance realized at the catalysts surface that deeply affects the ultimate process performance. Therefore, it should not be surprising that other more complex C-based functional materials from the literature, including those containing light-weight hetero-elements other than O, behave as our metal-free electrocatalysts or even outperform them in the $2e^-$ ORR process. The combination of light-dopants with highly defective carbon structures can generate a plethora of C-active sites to be engaged for the dioxygen activation/conversion. In principle, the greater the number of synthetic methodologies to the bottom-up preparation of light-weight hetero doped C-nanostructures (and the variety of surface groups containing the dopant), the greater the number of functionalities that will be claimed as the active sites for the process. Hence, *a never-ending story*!

Under this scenario, the exohedral functionalization with tailored groups appears as the long-sought solution for understanding the puzzling structure/reactivity relationship of O-containing carbon-based catalysts in ORR. It should put an end to this highly controversial matter, still under debate within the scientific community, highlighting the role of hydroxyl/phenol groups - classically overlooked from the literature - as key functionalities for the rational design of more performing electrocatalysts in the $2e^-$ ORR.

Experimental Section

General considerations: All manipulations were carried out using standard Schlenk-type techniques under nitrogen (N_2) or Argon (Ar) atmosphere. *o*DCB (*ortho*-dichlorobenzene) was dried following literature procedures[60] while dry acetonitrile (CH_3CN) was obtained by means of an MBraun Solvent Purification System. Unless otherwise stated, MWCNTs (>98% in C–Lot# MKBH5814V) and all other chemicals/solvents were purchased from Sigma-Aldrich and used as received. Sample sonication was accomplished with an Elma S15 Elmasonic sonicator bath (37 kHz) while CNTs filtration (whenever required by the synthetic procedure) was performed using PTFE filters (Whatman®) with 0.2 μm pore size.

Exhoedral functionalization of MWCNTs via aryldiazonium salt chemistry: In a typical procedure, MWCNTs (40 mg) were suspended in 32 mL of dry and degassed *o*DCB into a two-necked 100 mL flask and sonicated for 30 min. Afterwards, a degassed acetonitrile solution (16 mL) of the selected aniline (**1**-**4**, 0.86 mmol) and isopentyl nitrite (0.17 mL, 1.30 mmol) were added in small portions and the suspension was further sonicated for 10 min. The mixture was then heated at 80 °C for 14 h under magnetic stirring. The suspension was then cooled down to room temperature and the recovered solid (centrifugated) underwent four successive sonication/washing cycles [2 × $CH_3CO_2C_2H_5$, ethyl-acetate and 2 × CH_2Cl_2, dichloromethane). The resulting solid was finally suspended in dichloromethane, sonicated for 20 min and filtered through a 0.2 μm-pore PTFE filter. All work-up samples (**5**-**8**) were dried at 50 °C under vacuum to constant weight and stored in air at room temperature. For each functionalized material (**5**–**8**), a "*blank test*" was performed using identical reaction conditions and work-up procedures except for the use of the isopentyl nitrite as reagent.

Materials characterization and analyses conditions: *Thermogravimetric analysis* (TGA) was carried out under N_2 atmosphere (100 mL/min) on an EXSTAR Thermo Gravimetric Analyzer (TG/DTA) Seiko 6200 in the 40–700 °C range (heating rate: 5 °C/min). *Elemental analysis* (EA) was performed using a Thermo FlashEA 1112 Series CHNS analyzer and the average wt.% of each element was calculated over three independent runs. *X-ray Photoelectron Spectroscopy* (XPS) was performed in an ultra-high vacuum system (10^{-9}/10^{-10} mbar). The chamber was equipped with non-monochromatized dual anode (Al and Mg) and a hemispherical electron/ion energy analyzer (VSW mounting a 16-channel detector). The operating power of the used Al X-ray source was 120 W (12 kV and 10 mA) and photoelectrons were collected normal to the sample surface, maintaining the analyzer angle between analyzer axis and X-ray source fixed at 54.5°. An EtOH suspension of each sample was dropcasted on a slab of Bismuth foil. Samples were then kept under vacuum in the introduction chamber for at least 12 h in order to remove all adsorbed volatiles before acquiring XPS spectra in a fixed analyzer transmission mode with pass energy of 44.0 eV. The spectra were elaborated using the CasaXPS software. Shirley functions have been used to subtract the background. The deconvolution of the XPS spectra has been carried out employing a mixed Gaussian and Lorentzian function and the Binding energies (B.E.) were calibrated upon fixing the C1s sp^2 component at 284.8 eV.[52,56] The Brunauer–Emmett–Teller (BET) *specific surface area* (SSA) values were recorded on an ASAP 2020 Micromeritics instrument at −196 °C with liquid N_2 as adsorbent. All samples were activated at 120 °C for 24 h before measurements. Pore size distributions were evaluated by BJH method using the desorption branch of N_2 isotherms while micropore volume was estimated by t-plot method. *Acid-base titration* was accomplished according to slightly modified literature procedures.[45,47] In a typical measurement, 5 mg of the selected material were suspended in 7 mL of a standardized NaOH solution, sonicated for 30 min and stirred at rt for 48 h. After that, the suspension was filtered through a PTFE membrane and three aliquots of the filtrate were titrated with a standardized HCl solution. The surface acid content was therefore calculated as average value over three independent measurements. *EDX analysis* were carried out on a dual beam GAIA 3 FIB/SEM microscope equipped with an EDAX OCTANE ELECT SUPER detector. A 10 keV impinging electron beam was used as probe to generate the x-rays. Samples for analyses were suspended in 2-propanol upon sonication and then dropcasted on the surface of aluminum stubs. EDX quantification was performed on thicker particles by sampling an area of about 100 × 100 μm in order to better mediate the composition and minimize the influence of the Al beneath (not detected on the spectra). *High-resolution TEM* images were acquired using a Thermo-Fisher F200X G2 HR-TEM with a beam energy of 200 keV. Samples were prepared on 200 mesh holey-carbon supported copper grids by evaporative drop-casting of sonicated CNT suspensions in 2-propanol.

Electrochemical measurements: Rotating ring-disk electrode (RRDE) measurements were performed on a Pine AFE6R2GCPT instrument equipped with a glassy carbon disk (Ø 5 mm, A = 0.196 cm^2) and a Pt ring (A = 0.11 cm^2), using a Bio-Logic SP-300 potentiostat and the EC-Lab 11.32 software. CNTs samples (5 mg) were dispersed in 750 μL of ultrapure water, 250 μL of 2-propanol and 50 μL of a Nafion® solution (5 wt.% in alcohols and water) and sonicated for 30–45 min to obtain a homogeneous ink. Afterwards, 17 μL of each suspension was dropcasted on the disk (Working Electrode, catalyst charge: 414 μg/cm^2) and left to dry at room temperature. The as-prepared WE was employed for electrochemical measurements in a three-electrode cell with an Ag/AgCl/$KCl_{sat.}$ electrode and a graphite rod as the reference (RE) and the counter electrode (CE), respectively, with two compartments separated by a porous glass membrane used for housing the WE and CE. Linear Sweep Voltammetry (LSV) measurements were carried out in a 0.1 M KOH solution saturated with O_2 at a scan rate of 10 mV/s in the potential range from −0.9 to + 0.2 V vs. Ag/AgCl/KClsat and then referred to the reversible hydrogen electrode (RHE) according to the following equation: $E_{RHE} = E_{Ag/AgCl/KClsat.} + 0.197 + 0.0592pH$. Background currents, measured under saturated N_2 conditions, were subtracted from the respective curves to eliminate all capacitive contributions. A long-term cycling RRDE test on **5** was recorded in the 0.1 ÷ 0.9 V vs. RHE potentials range with a scan rate of 200 mV s^{-1} and an electrode spin rate of 1600 rpm in 0.1 M KOH at 25 °C. H_2O_2 selectivity was measured either from currents recorded at the Pt ring (held at a potential of + 1.2 V vs. RHE during the whole electrochemical test) (eqs. 5–6) of the RRDE electrode and calculated from the number of exchanged electrons (n) *per* O_2 molecule as obtained by the Koutecky-Levich equation [Eq. (7)].

$$H2O2\ (\%) = \ 200^* \frac{I_R/N}{I_D + I_R/N} \tag{5}$$

$$n = \ 4^* \ \frac{I_D}{I_D + I_R/N} \tag{6}$$

where I_R and I_D are the ring and the disk current values, respectively, and N is the ring collection efficiency (0.256).

$$\frac{1}{J} = \frac{1}{J_K} + \frac{1}{nK_f\sqrt{f}} \text{ with}$$
$$K_f = 0.2FC_0D_0^{2/3}\nu^{-1/6} \tag{7}$$

where J is the current density (mA/cm^2), J_K is the kinetic current density (mA/cm^2), n is the number of exchanged electrons, F is the Faraday constant, C_0 is the O_2 concentration in solution (1.15 × 10^{-3} mol/dm^3), D_0 is the oxygen diffusion coefficient (1.95 × 10^{-5} cm^2/s), f is the electrode angular rotation rate (rpm), ν is the electrolyte kinematic viscosity (0.008977 cm^2/s).[61] The average number of exchanged electrons (n) during the ORR was extrapolated from the slop of the J^{-1} vs. $f^{-1/2}$ plot at a specific potential value.

Computational details: A CNT simplified model structure made of 42 C atoms supporting the exohedral dangling groups has been built and fully optimized with the Vienna ab initio simulation package (VASP),[62–64] using a generalized gradient approximation (GGA) and the Perdew–Burke–Ernzerhof (PBE) functional[65] to express the exchange-correlation potential. A 3 × 3 × 3 k-points mesh and 450 eV energy cutoff were used for structure relaxation.

The ionic relaxation during optimization was carried out under conventional energy (10^{-5} eV) and force convergence criteria were set to 0.02 eV Å^{-1}. To avoid the interaction between periodic images, the distance between neighboring cells is set to ~12 Å. The Bader charge analysis[66] was performed on the optimized structures using the same computational setup.

Acknowledgements

G. G. and C. P.-H. thank the TRAINER project (Catalysts for Transition to Renewable Energy Future) of the "Make our Planet Great Again" program (Ref. ANR-17-MPGA-0017) for support. G. G. and G. T. would also like to thank the Italian MIUR through the PRIN 2017 Project Multi-e (20179337R7) "Multielectron transfer for the conversion of small molecules: an enabling technology for the chemical use of renewable energy" for financial support to this work. Y. L. and G. G. finally thank the CAS President's International Fellowship Initiative (PIFI) program for support. We also thank B. Cortigiani for his assistance in using MatchLab Interdepartmental Research Unit (Univ. of Florence).

Conflict of Interests

The authors declare no conflict of interest.

Data Availability Statement

The data that support the findings of this study are available in the supplementary material of this article.

Keywords: 2e$^-$ oxygen reduction reaction · carbon nanomaterials functionalization · electrocatalyst surface chemical engineering · hydrogen peroxide production · metal-free electrocatalysts,

[1] R. L. Myers, *The 100 Most Important Chemical Compounds*, Greenwood Press, London, **2007**,.
[2] Y. Pang, H. Xie, Y. Sun, M.-M. Titirici, G.-L. Chai, *J. Mater. Chem. A* **2020**, *8*, 24996–25016.
[3] R. J. Lewis, G. J. Hutchings, *ChemCatChem* **2019**, *11*, 298–308.
[4] Y. Yamada, S. Fukuzumi, *ChemElectroChem* **2016**, *3*, 1978–1989.
[5] J. M. Campos-Martin, G. Blanco-Brieva, J. L. G. Fierro, *Angew. Chem. Int. Ed.* **2006**, *45*, 6962–6984.
[6] C. Xia, S. Back, S. Ringe, K. Jiang, F. Chen, X. Sun, S. Siahrostami, K. Chan, H. Wang, *Nat. Catal.* **2020**, *3*, 125–134.
[7] W. Zhou, L. Xie, J. Gao, R. Nazari, H. Zhao, X. Meng, F. Sun, G. Zhao, J. Ma, *Chem. Eng. J.* **2021**, *410*, 128368.
[8] S. C. Perry, D. Pangotra, L. Vieira, L.-I. Csepei, V. Sieber, L. Wang, C. Ponce de Leon, F. C. Walsh, *Nat. Chem. Rev.* **2019**, *3*, 442–458.
[9] Z. Deng, C. Ma, S. Yan, K. Dong, Q. Liu, Y. Luo, Y. Liu, J. Du, X. Sun, B. Zheng, *J. Mater. Chem. A* **2021**, *9*, 20345–20349.
[10] K. Dong, J. Liang, Y. Ren, Y. Wang, Z. Xu, L. Yue, T. Li, Q. Liu, Y. Luo, Y. Liu, S. Gao, M. S. Hamdy, et al., *J. Mater. Chem. A* **2021**, *9*, 26019–26027.
[11] I. Eryazici, N. Ramesh, C. Villa, *MRS Bull.* **2021**, *46*, 1197.
[12] G. Papanikolaou, G. Centi, S. Perathoner, P. Lanzafame, *ACS Catal.* **2022**, *12*, 2861–2876.
[13] Y. Li, Q. Li, H. Wang, L. Zhang, D. P. Wilkinson, J. Zhang, *Electrochem. Energy Rev.* **2019**, *2*, 518–538.
[14] Y.-L. Zhang, K. Goh, L. Zhao, X.-L. Sui, X.-F. Gong, J.-J. Cai, Q.-Y. Zhou, H.-D.–. Zhang, L. Li, F.-R. Kong, D.-M. Gu, Z.-B. Wang, *Nanoscale* **2020**, *12*, 21534–21559.
[15] S. Siahrostami, A. Verdaguer-Casadevall, M. Karamad, D. Deiana, P. Malacrida, B. Wickman, M. Escudero-Escribano, E. A. Paoli, R. Frydendal, T. W. Hansen, I. Chorkendorff, I. E. L. Stephens, et al., *Nat. Mater.* **2013**, *12*, 1137–1143.
[16] A. Verdaguer-Casadevall, D. Deiana, M. Karamad, S. Siahrostami, P. Malacrida, T. W. Hansen, J. Rossmeisl, I. Chorkendorff, I. E. L. Stephens, *Nano Lett.* **2014**, *14*, 1603–1608.
[17] J. S. Jirkovský, I. Panas, E. Ahlberg, M. Halasa, S. Romani, D. J. Schiffrin, *J. Am. Chem. Soc.* **2011**, *133*, 19432–19441.
[18] Z. Zheng, Y. H. Ng, D.-W. Wang, R. Amal, *Adv. Mater.* **2016**, *28*, 9949–9955.
[19] S. Wu, L. Yu, G. Wen, Z. Xie, Y. Lin, *J. Energy Chem.* **2021**, *58*, 318–335.
[20] G. Tuci, M. Pilaski, H. Ba, A. Rossin, L. Luconi, S. Caporali, C. Pham-Huu, R. Palkovits, G. Giambastiani, *Adv. Funct. Mater.* **2017**, *27*, 1605672.
[21] L. Yang, J. Shui, L. Du, Y. Shao, J. Liu, L. Dai, Z. Hu, *Adv. Mater.* **2019**, *31*, 1804799.
[22] C. Hu, Q. Dai, L. Dai, *Cell Rep. Phys. Sci.* **2021**, *2*, 100328.
[23] X. C. Duan, J. T. Xu, Z. X. Wei, J. M. Ma, S. J. Guo, S. J. Wang, H. K. Liu, S. X. Dou, *Adv. Mater.* **2017**, *29*, 1701784.
[24] Y. Zhou, G. Chen, J. Zhang, *J. Mater. Chem. A* **2020**, *8*, 20849–20869.
[25] T.-P. Fellinger, F. Hasché, P. Strasser, M. Antonietti, *J. Am. Chem. Soc.* **2012**, *9*, 4072–4075.
[26] D. Iglesias, A. Giuliani, M. Melchionna, S. Marchesan, A. Criado, L. Nasi, M. Bevilacqua, C. Tavagnacco, F. Vizza, M. Prato, P. Fornasiero, *Chem* **2018**, *4*, 106–123.
[27] K. Zhao, Y. Su, X. Quan, Y. Liu, S. Chen, H. Yu, *J. Catal.* **2018**, *357*, 118–126.
[28] K. Li, J. Liu, J. Li, Z. Wan, *Chemosphere* **2018**, *193*, 800–810.
[29] S. Chen, Z. Chen, S. Siahrostami, D. Higgins, D. Nordlund, D. Sokaras, T. R. Kim, Y. Liu, X. Yan, E. Nilsson, R. Sinclair, J. K. Nørskov, et al., *J. Am. Chem. Soc.* **2018**, *140*, 7851–7859.
[30] L. Li, C. Tang, Y. Zheng, B. Xia, X. Zhou, H. Xu, S.-Z. Qiao, *Adv. Energy Mater.* **2020**, *10*, 2000789.
[31] Z. Lu, G. Chen, S. Siahrostami, Z. Chen, K. Liu, J. Xie, L. Liao, T. Wu, D. Lin, Y. Liu, T. F. Jaramillo, J. K. Nørskov, et al., *Nat. Catal.* **2018**, *1*, 156–162.
[32] G.-F. Han, F. Li, W. Zou, M. Karamad, J.-P. Jeon, S.-W. Kim, S.-J. Kim, Y. Bu, Z. Fu, Y. Lu, S. Siahrostami, J.-B. Baek, *Nat. Commun.* **2020**, *11*, 2209.
[33] Z. Pan, K. Wang, Y. i. Wang, P. Tsiakaras, S. Song, *Appl. Catal. B* **2018**, *237*, 392–400.
[34] H. W. Kim, M. B. Ross, N. Kornienko, L. Zhang, J. Guo, P. Yang, B. D. McCloskey, *Nat. Catal.* **2018**, *1*, 282–290.
[35] S. Chen, T. Luo, K. Chen, Y. Lin, J. Fu, K. Liu, C. Chai, Q. Wang, H. Li, X. Li, J. Hu, H. Li, et al., *Angew. Chem. Int. Ed.* **2021**, *60*, 16607–16614.
[36] Y. Pang, K. Wang, H. Xie, Y. Sun, M.-M. Titirici, G.-L. Chai, *ACS Catal.* **2020**, *10*, 7434–7442.
[37] D. San Roman, D. Krishnamurthy, R. Garg, H. Hafiz, M. Lamparski, N. T. Nuhfer, V. Meunier, V. Viswanathan, T. Cohen-Karni, *ACS Catal.* **2020**, *10*, 1993–2008.
[38] F. Sun, C. Yang, Z. Qu, W. Zhou, Y. Ding, J. Gao, G. Zhao, D. Xing, Y. Lu, *Appl. Catal. B* **2021**, *286*, 119860.
[39] K. Dong, J. Liang, Y. Wang, Z. Xu, Q. Liu, Y. Luo, T. Li, L. Li, X. Shi, A. M. Asiri, Q. Li, D. Ma, et al., *Angew. Chem. Int. Ed.* **2021**, *60*, 10583–10587.
[40] J. Lee, Y. Lee, J. S. Lim, S. W. Kim, H. Jang, B. Seo, S. H. Joo, Y. J. Sa, *Nanoscale* **2023**, *15*, 195–203.
[41] X. Lu, D. Wang, K.-H. Wu, X. Guo, W. Qi, *J. Colloid Interface Sci.* **2020**, *573*, 376–383.
[42] G. Tuci, L. Luconi, A. Rossin, G. Giambastiani, *Chimia* **2017**, *71*, 568–572.
[43] G. Tuci, A. Rossin, X. Zhang, C. Pham-Huu, G. Giambastiani, *Curr. Opin. Green Sustain. Chem.* **2022**, *33*, 100579.
[44] G. Tuci, C. Zafferoni, P. D'Ambrosio, S. Caporali, M. Ceppatelli, A. Rossin, T. Tsoufis, M. Innocenti, G. Giambastiani, *ACS Catal.* **2013**, *3*, 2108–2111.
[45] G. Tuci, C. Zafferoni, A. Rossin, A. Milella, L. Luconi, M. Innocenti, L. Truong Phuoc, C. Duong-Viet, C. Pham-Huu, G. Giambastiani, *Chem. Mater.* **2014**, *26*, 3460–3470.
[46] G. Tuci, C. Zafferoni, A. Rossin, L. Luconi, A. Milella, M. Ceppatelli, M. Innocenti, Y. Liu, C. Pham-Huu, G. Giambastiani, *Catal. Sci. Technol.* **2016**, *6*, 6226–6236.
[47] G. Tuci, L. Luconi, A. Rossin, E. Berretti, H. Ba, M. Innocenti, D. Yakhvarov, S. Caporali, C. Pham-Huu, G. Giambastiani, *ACS Appl. Mater. Interfaces* **2016**, *8*, 30099–30106.

[48] G. Tuci, J. Filippi, H. Ba, A. Rossin, L. Luconi, C. Pham-Huu, F. Vizza, G. Giambastiani, *J. Mater. Chem. A* **2018**, *6*, 16382–16389.
[49] G. Tuci, A. Rossin, L. Luconi, C. Pham-Huu, S. Cicchi, H. Ba, G. Giambastiani, *Catal. Sci. Technol.* **2017**, *7*, 5833–5837.
[50] J. L. Bahr, J. M. Tour, *Chem. Mater.* **2001**, *13*, 3823–3824.
[51] M. E. Lipinska, S. L. H. rebelo, M. F. R. Pereira, J. A. N. F. Gomes, C. Freire, J. L. Figueiredo, *Carbon* **2012**, *50*, 3280–3294.
[52] B. Yu, X. Wang, X. Qian, W. Xing, H. Yang, L. Ma, Y. Lin, S. Jiang, L. Song, Y. Hu, S. Lo, *RSC Adv.* **2014**, *4*, 31782–31794.
[53] J. L. Figueiredo, M. F. R. Pereira, M. M. A. Freitas, J. J. M. Orfao, *Carbon* **1999**, *37*, 1379–1389.
[54] V. Datsyuk, M. Kalyva, K. Papagelis, J. Parthenios, D. Tasis, A. Siokou, I. Kallitsis, C. Galiotis, *Carbon* **2008**, *46*, 833–840.
[55] Y. Lin, X. Sun, D. S. Su, G. Centi, S. Perathoner, *Chem. Soc. Rev.* **2018**, *47*, 8438–8473.
[56] J. S. Stevens, C. R. Seabourne, C. Jaye, D. A. Fischer, A. J. Scott, S. L. M. Schroeder, *J. Phys. Chem. B* **2014**, *118*, 12121–12129.
[57] K. S. W. Sing, D. H. Everett, R. A. W. Haul, L. Moscou, R. A. Pierotti, J. Rouquérol, *Pure Appl. Chem.* **1985**, *57*, 603–619.
[58] R. Zhou, Y. Zheng, M. Jaroniec, S.-Z. Qiao, *ACS Catal.* **2016**, *6*, 4720–4728.
[59] W. Zhou, L. Rajic, X. Meng, R. Nazari, Y. Zhao, Y. Wang, J. Gao, Y. Qin, A. N. Alshawabkeh, *Chem. Eng. J.* **2019**, *364*, 428–439.
[60] D. D. Perrin, W. L. F. Armarego, D. R. Perrin, *Purification of Laboratory Chemicals, Vol. 1*, 2nd ed., **1980**,.
[61] Y. Wang, D. Zhang, H. Liu, *J. Power Sources* **2010**, *195*, 3135–3139.
[62] G. Kresse, J. Furthmüller, *Comput. Mater. Sci.* **1996**, *6*, 15–50.
[63] G. Kresse, J. Furthmüller, *Phys. Rev. B* **1996**, *54*, 11169–11186.
[64] G. Kresse, J. Hafner, *Phys. Rev. B* **1993**, *47*, 558–561.
[65] J. P. Perdew, A. Ruzsinszky, G. I. Csonka, O. A. Vydrov, G. E. Scuseria, L. A. Constantin, X. Zhou, K. Burke, *Phys. Rev. Lett.* **2008**, *100*, 136406.
[66] R. Bader, *Atoms in Molecules: A Quantum Theory*, Oxford University Press, **1990**, 456.

Manuscript received: March 31, 2023
Accepted manuscript online: May 7, 2023
Version of record online: June 16, 2023